

Modeling Immune-Mediated Tumor Growth and Treatment

Lisette de Pillis and Ami Radunskaya

Abstract The immune response is an important factor in the progression of cancer, and this response has been harnessed in a variety of treatments for a range of cancers. In this chapter we develop mathematical models that describe the immune response to the presence of a tumor. We then use these models to explore a variety of immunotherapy treatments, both alone and in combination with other therapies.

Keywords Tumor-immune interactions • Effector cell kill rate • Therapy optimization • Agent-based models • Immune response kinetics

1 Introduction

The simplest model of tumor growth assumes that cells undergo mitosis at a constant rate, resulting in a tumor population that grows exponentially. However, it is quickly apparent that this model is not consistent with clinical observation. As a thought experiment, consider a breast cancer cell, which is approximately 20 microns in diameter. If we assume a doubling time of two days, then after 26 doublings or 52 days, this single cell will have produced a mass of approximately 67 million cells, with a diameter of 8 mm—in other words a detectable tumor mass. After another 18 doublings or 88 days after the single cancer cell started dividing, the mass would be the size of a beach ball (of radius 25 cm).

Clinicians knew from experience that, in general, this was not a correct description of tumor growth, even in the absence of treatment. Tumor growth could be limited by many factors, an obvious one being a limited supply of nutrients, and several early mathematical models were proposed that account for the slowing

L.G. de Pillis
Harvey Mudd College, Claremont, CA 91711, USA
e-mail: depillis@hmc.edu

A.E. Radunskaya (✉)
Pomona College, Claremont, CA 91711, USA
e-mail: aradunskaya@pomona.edu

of tumor growth as a result of limits on the ability of the vasculature to deliver nutrients [10, 42, 55]. There was also ample evidence that the immune system plays a significant role in the containment of tumors.

The exact role of the immune system in fighting cancer is not known, although as early as 1908, scientists proposed that the immune system could prevent the progression of many cancers. In particular, in that year, Nobel laureate Paul Ehrlich deduced that, without the immune system's intervention, there would be many more cases of cancer than we observe [25]. Throughout the past century, the "immunosurveillance" hypothesis was tested and retested, with experimental results sometimes supporting the hypothesis, sometimes rejecting it [24]. In the past two decades, the overwhelming majority of evidence is in favor of Ehrlich's hypothesis, and researchers are now seeking ways to enhance the ability of the immune system to stop the progression of the disease [26].

One of the earliest attempts to harness the immune system's response was made by an oncologist, William B. Coley, in the late 1800s, who noticed that some of his patients with what he thought was incurable cancer would improve when they simultaneously had an infection. He manufactured a mixture of dead bacteria, and experimentally administered the brew, known as "Coley's toxins," to patients with inoperable tumors. This treatment was successful enough to encourage other doctors to follow suit throughout the following decades [56]. Other immunotherapy treatments for cancer include stem cell transplants, introduced in the 1950's, and the administration of immune-stimulating cytokines. A stem cell transplant involves harvesting immune cells from the bone marrow of healthy individuals and transferring them to patients with leukemia. The administration of immune-stimulating cytokines is a technique that was pioneered and developed by Dr. Steven Rosenberg to treat patients with melanoma [50]. For an excellent review of cancer immunotherapies, see [3].

The role of the immune response in the control of cancerous cells also caught the interest of the mathematical community. Over the past twenty years, physicists and applied mathematicians have developed mathematical models that describe the interactions between tumor cells and immune cells in an attempt to understand the mechanisms behind observed behavior and to help clinicians design effective treatments. The earlier models consider tumor cells and immune cells at the population level [33, 36, 44, 52]. For an excellent survey of these early models see the book [1]. Later models include spatial effects [4, 5, 41] or focus on optimization of specific immunotherapy treatments [6, 35]. General frameworks have been developed from a systems perspective that are applicable to a variety of specific situations [19, 20]. This chapter is not intended to be an overview of this impressive body of work; the interested reader is referred to the texts cited here and the references therein. Rather, we follow our own trajectory of investigation and discovery, presenting several models of tumor-immune interactions that illustrate a variety of approaches to understanding the progression of the disease and to harnessing the immune response in the context of treatment.

This chapter is organized as follows. In Sect. 2 we develop the simplest model of the immune response, which uses two ordinary differential equations to describe two competing populations: the immune cells and the tumor cells. We add chemotherapy

to this simple model to illustrate the complexity in the resulting dynamics and to demonstrate *in silico* the importance of including the immune response in the design of treatment strategies. We add more realism to the model in Sect. 3 by distinguishing between the innate and the adaptive immune responses and describe several types of modeling techniques that can be used to explore this distinction. In the final section of the chapter, Sect. 4, we discuss immunotherapies, and give several examples of mathematical models that can be used to investigate immunotherapeutic protocols.

2 The Immune Response as One Population of Effector Cells

The immune system is a complex network of interacting cells, proteins and chemicals. This network consists of excitatory and inhibitory connections, positive and negative feedback loops, and delays. In the simplest mathematical model of tumor-immune interactions, we only consider those immune cells that have the ability to destroy antigen, or foreign cells. These include natural killer (NK) cells, cytotoxic T-cells (CTL) such as $CD8^+$ cells, macrophages, and other scavenger cells. As a first model, we lump all of these killer cells into one population called **effector cells**. We imagine that we are considering a small volume of tissue containing a tumor, we consider the tumor to be one homogeneous population of cells, and we assume that the interaction between tumor and effector cells can be described as an *average* affect. If the number of cells in each of the populations is large, we can describe the population as a continuum, and we can describe the evolution of the average using differential equations. We also include a population of normal host cells in this model, as a proxy for overall “well-being.” Since a tumor cannot grow without bound, we assume that, in the absence of an immune response, the tumor will grow to some maximum size determined by the available nutrients. We assume the same for the normal cells. Several functional forms are used to model self-limiting growth in the literature, for example, logistic, Gompertz, or von Bertalanffy. In this formulation we use a logistic growth law for both normal and tumor cells. We note, however, that other growth laws produce qualitatively similar results. Further details of this model and an analysis of its long-term behavior can be found in [14] and [15].

We let $I(t)$ denote the number of effector immune cells at time t , $T(t)$ the number of tumor cells at time t , and $N(t)$ the number of normal, or host, cells at time t . A graphical representation of the model interactions is shown in Fig. 1.

The source of the immune cells is considered to be outside of the system, and we let s denote the constant influx of innate effector cells that would be present in the absence of a tumor. Furthermore, in the absence of any tumor, the cells will die off at a per capita rate d_1 , resulting in a long-term population size of s/d_1 cells. Thus, immune cell proliferation will never suffer from crowding.

The presence of tumor cells stimulates the immune response, represented by the dashed arrow in the diagram. For biological realism, we assume here a saturation

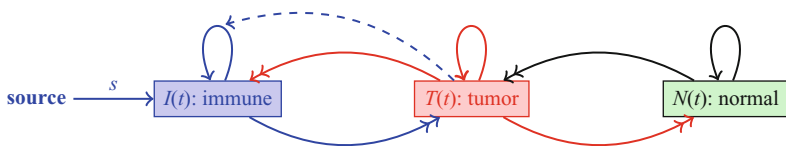


Fig. 1 A graphical representation of a population model of tumor-immune interactions, with three populations: immune effector cells (I), tumor cells (T), and normal cells (N). *Solid lines* indicate direct interactions, and *dashed lines* indicate indirect interactions. *Single arrow heads* denote a positive interaction, while *double arrow heads* denote an inhibitory interaction

limited effect. Furthermore, the reaction of immune cells and tumor cells can result in either the death of tumor cells or the inactivation of the immune cells, represented by two double-headed arrows.

The closed loop arrows on the tumor and normal cell population nodes represent normal growth and decay, which follows a logistic law. In addition there are two terms representing the competition between tumor and host cells, shown also as double-headed arrows in the diagram. Putting all the terms together gives the following system of ordinary differential equations:

$$\begin{aligned}
 \dot{N} &= r_2 N(1 - b_2 N) - c_4 TN, \\
 \dot{T} &= r_1 T(1 - b_1 T) - c_2 IT - c_3 TN, \\
 \dot{I} &= s + \frac{\rho IT}{\alpha + T} - c_1 IT - d_1 I.
 \end{aligned}
 \tag{1}$$

As shown in [15], this system has one “tumor-free” equilibrium at $(1/b_2, 0, s/d_1)$ and two “dead” equilibria, where the normal cell population is zero. Furthermore, the system can have one, two, or three “co-existing” equilibria, where all of the cell populations are nonzero, depending on the values of the parameters. Thus, in some parameter regimes, the system is *multistable*, where several stable equilibria exist at the same time, so that the long-term behavior of the system is determined by the initial conditions. We note that the concept of multistability is one of the few new ideas that biomathematics was able to offer the biomedical research community.

If the tumor-free equilibrium is stable, then small tumors will be eradicated by the immune system. A linearized stability analysis shows that this occurs when the *resistance coefficient* is larger than the intrinsic growth rate of the tumor, i.e., when

$$\frac{c_2 s}{d_1} + c_3 > r_1.$$

If a patient has a detectable tumor that is progressing, then we can assume that the tumor-free equilibrium is unstable. Two bifurcation diagrams are shown in Fig. 2.

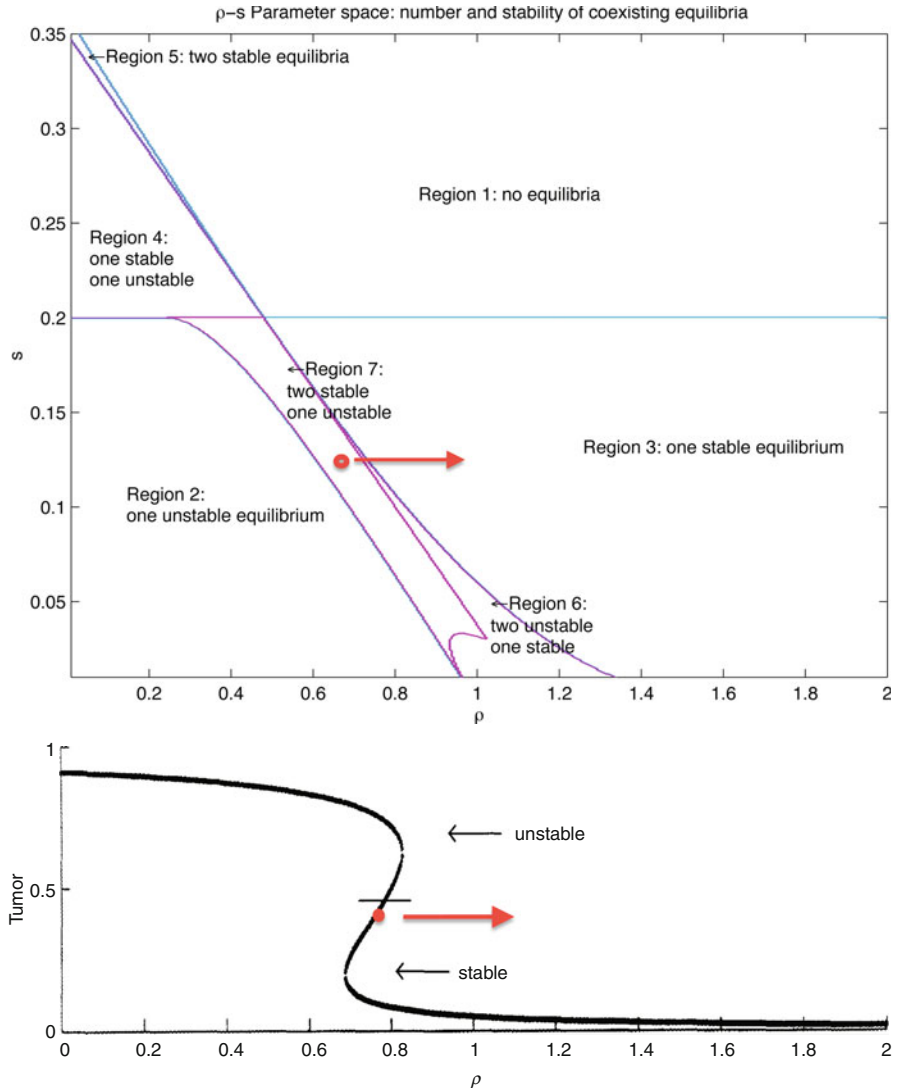


Fig. 2 Bifurcation diagram showing how changes in the immune source (s) and recruitment (ρ) parameters affect the number and stability of equilibria with nonzero tumor values. Note that the tumor-free equilibrium is not shown here: it is assumed to be unstable if there is a tumor. The red arrow indicates movement through the diagram as a result of a hypothetical treatment that enhances the immune response, such as the administration of interleukin 2 (IL2). Upper graph: Number and type of co-existing equilibria as a function of source rate, s , and immune response, ρ . Lower graph: Tumor cell populations at the equilibria as a function of the immune response rate, ρ . Stability of equilibria is indicated. Movement is from Region 2 through Regions 7 and 6 and finally into Region 3: as ρ increases from 0.1 to 2.0. Source rate $s = .12$, tumor populations as fraction of carrying capacity. See [15] for details

We can interpret these diagrams in the context of immunotherapy treatments as follows: treatment should move the system into a regime where it is attracted to a small, presumably harmless, tumor. If a patient has a detectable tumor that is progressing, we can assume that it is *not* in the basin of attraction of a stable, small-tumor equilibrium. Suppose the system is in Region 7, where it will be attracted to a relatively large tumor equilibrium (the dot in both graphs in Fig. 2). By administering cytokines that increase the immune response or by giving a vaccine that increased the immunogenicity of the tumor, the parameter ρ could be increased, moving the system to the right in the bifurcation diagrams (denoted by the arrows in both graphs). The system would then be in the basin of attraction of a relatively small tumor equilibrium, and the tumor would regress without further treatment.

We can also learn something about the effects of uncertainty in the environment by looking at the bifurcation diagram. For example, suppose the system is near the right boundary of Region 7 in Fig. 2, for example, near the point $s = .17$, $\rho = .6$. In this case, small fluctuations in the parameter s , the influx rate of effector cells in the absence of a tumor, could cause the system to move into Region 3. A reverse saddle-node bifurcation occurs where one stable equilibrium and one unstable equilibrium disappear, and the system would move towards the one remaining stable equilibrium. In this case, this would be beneficial, since the remaining equilibrium is at a point in state space with a small tumor population. The effect of stochastic fluctuations in the parameters has been discussed in the context of tumor-immune models in, for example, [7], and the effects of random fluctuations on resistance to chemotherapy is treated nicely in [21].

2.1 *The Immune Response and Chemotherapy*

In a scenario known as “Jeff’s phenomenon,” it has been clinically observed that tumors treated with cytotoxic chemotherapy can respond in a non-intuitive way. For some patients, after one treatment the tumor will shrink, and after another it might continue to grow, resulting in a temporal oscillation that is asynchronous with the chemotherapy. This phenomenon is reported in [59], where it is argued that this asynchronicity cannot be explained solely by acquired drug resistance. We hypothesize that it is the interaction of the chemotherapy with the immune response that could explain Jeff’s phenomenon and test the hypothesis by adding a chemotherapeutic term to the model.

We assume that the rate of change of the concentration of drug at the tumor site, $u(t)$, can be described by a time-varying input function, $v(t)$, representing the administration of the drug, and by an elimination rate, d_1 . We also assume that the drug kills all three types of cells in the model at a saturating rate, but that it acts preferentially on the more quickly dividing tumor cells and immune cells than on the normal host cells. A graphical representation of the system is shown in Fig. 3, with edges terminating in open circles denoting an inhibitory (killing) effect.

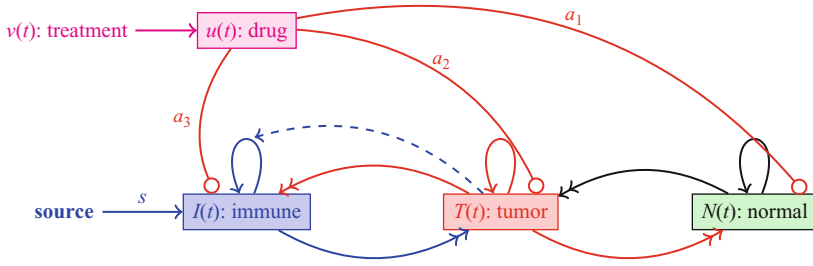


Fig. 3 A graphical representation of the model with chemotherapy. *Solid lines* represent direct interactions, with single arrowheads representing cooperative interactions, double arrowheads representing competitive interactions, and open circles representing a killing effect. *Dashed lines* represent interactions that affect the rate of another interaction

These assumptions result in the following system of equations (see [15] for parameter values and more details):

$$\begin{aligned}
 \dot{N} &= r_2 N(1 - b_2 N) - c_4 TN - a_1(1 - e^{-u})N, \\
 \dot{T} &= r_1 T(1 - b_1 T) - c_2 IT - c_3 TN - a_2(1 - e^{-u})T, \\
 \dot{I} &= s + \frac{\rho IT}{\alpha + T} - c_1 IT - d_1 I - a_3(1 - e^{-u})I, \\
 \dot{u} &= v(t) - d_1 u.
 \end{aligned}
 \tag{2}$$

where $a_1 < a_3 < a_2$. A simulation of this model demonstrating Jeff’s phenomenon is shown in Fig. 4. Thus, the immune response could play a role in the delayed response of some patients to cytotoxic chemotherapy. This simple model also suggests that a close monitoring of the state of the cellular immune response could help in designing more effective treatment protocols.

With the relatively simple model given by Equation 2, we can attempt to answer the question: what is the best treatment regimen for a patient with a specific parameter set? As a first step, we must define what we mean by “best.” One criterion might be “the one that minimizes tumor size at the end of treatment” and another might be “the one that is least toxic.” Once the criteria are settled, optimization techniques can be applied to the system to propose effective treatment protocols. For example, suppose we wish to minimize the tumor burden after 45 days of treatment, while keeping the tumor population as low as possible and keeping the

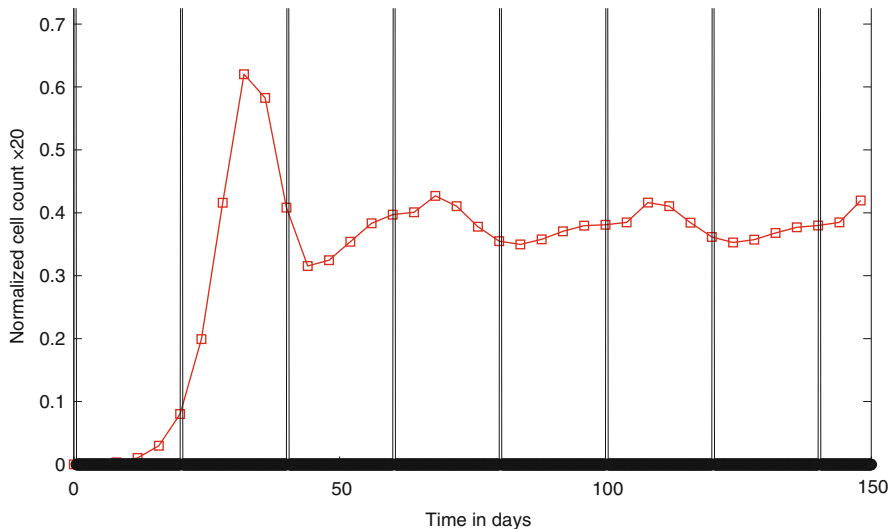


Fig. 4 Simulation of the model in system 2 demonstrates a possible role of the immune response in an asynchronous response to chemotherapy. Vertical lines show the simulated bolus injections of the drug, administered every 21 days

level of normal cells above 75% of their normal value (a measure of toxicity). In terms of an optimization problem, we want to find the function $v(t)$, representing the administration of the drug, that minimizes the following *cost* function, where t_f is the total time of treatment.

$$J(v(t)) = w_1 T(t_f) + w_2 \int_0^{t_f} T(t) dt + w_3 \max_{t \in (t_0, t_f)} T(t), \quad (3)$$

where w_i are weighting constants. Note that three terms were required in the cost function: the first reflects our desire to minimize the tumor at the end of treatment, t_f . The second reflects our desire to minimize the total tumor present over the course of treatment, and the third term puts a penalty on any treatment that results in a large tumor at any point. The omission of either of the final two terms yields solutions with tumor populations that grow very large for a short period of time. The weighting of the three terms also yields qualitatively different results. For the set of experiments we present here, we set $w_1 = 1500$, $w_2 = 150$, $w_3 = 1000$, but other weightings might be preferred, depending on the type of tumor.

To reflect our desire to avoid excessive toxicity, we introduce a *constraint* function:

$$N(t) \geq 0.75, \quad 0 \leq t \leq t_f, \quad (4)$$

where the host cell population, $N(t)$, is scaled to a fraction of its normal value. Additional constraints are that all state variables must satisfy Equation 2 and that both the rate of drug input and the total amount of drug administered are bounded: $0 \leq v(t) \leq \max_v$, $0 \leq \int_0^{t_f} v(t) dt \leq v_{TOT}$.

This optimization problem can be solved using a variety of available techniques. In Fig. 5 we compare simulations using a traditional, “pulsed” protocol, where the drug is administered over short (12 h) periods, repeated every 2 days for 40 treatments (so the last treatment ends midday on Day 80). In this experiment, we simulate a patient with a relatively weak initial immune system ($I(0) = .1$) and the simulation shows that the traditional pulsed treatment is ineffective in the long term: once treatment stops, the tumor continues to grow, and the disease progresses. In the right panel of Fig. 5 we show a solution obtained using a direct collocation method, DIRCOL [57]. We required that the total amount of drug administered be no more than the total in the traditional case, so $v_{TOT} = \sum_{n=1}^{40} \int_0^{.5} 1 dt = 20$. The optimized protocol suggests that the drug be administered over longer periods of time, on the order of days, with irregularly spaced treatments. In fact, it suggests one very short pulse of chemo at Day 125. With this treatment the tumor burden is driven to near zero by Day 70, and it remains there for the duration of the simulation. It is worth emphasizing that the only difference between the two treatments is the *timing* of the doses: the total amount of drug, and the maximum drug given are the same.

There are many possible optimization questions that could be asked in this setting. For example, it is possible that, by adding the total amount of drug used to the cost functional, one could find treatment protocols that are equally effective but that use less drug. Or it might be desirable to introduce a penalty term that curbs the destruction of the immune population. In Sect. 4 we will explore other optimization techniques and results in the context of designing cancer vaccines.

3 The Innate and Adaptive Immune Response

The human body has a huge army of defender cells, generally known as *white blood cells* (WBC) or *leukocytes*. It creates approximately a billion of these cells each day. A subset of these leukocytes are *lymphocytes*, which comprise 20–30% of the WBC. In this section we will focus on two types of lymphocytes: the natural killer (NK) lymphocytes and the cytotoxic T lymphocytes (CTLs). Both of these cells are *cytotoxic*, meaning that they kill antigen or “nonself” cells. However, they belong to two different arms of the immune response: NK cells belong to the *innate* immune system. They form part of the immune system’s regular patrol, and they are activated to *lyse*, or kill, cells that they encounter when that cell does not have a high expression level of certain molecules known as MHC I (major histocompatibility complex class I). The CTLs are part of the *adaptive* immune system. These cells originate from stem cells that then migrate to the thymus (hence the “T”).

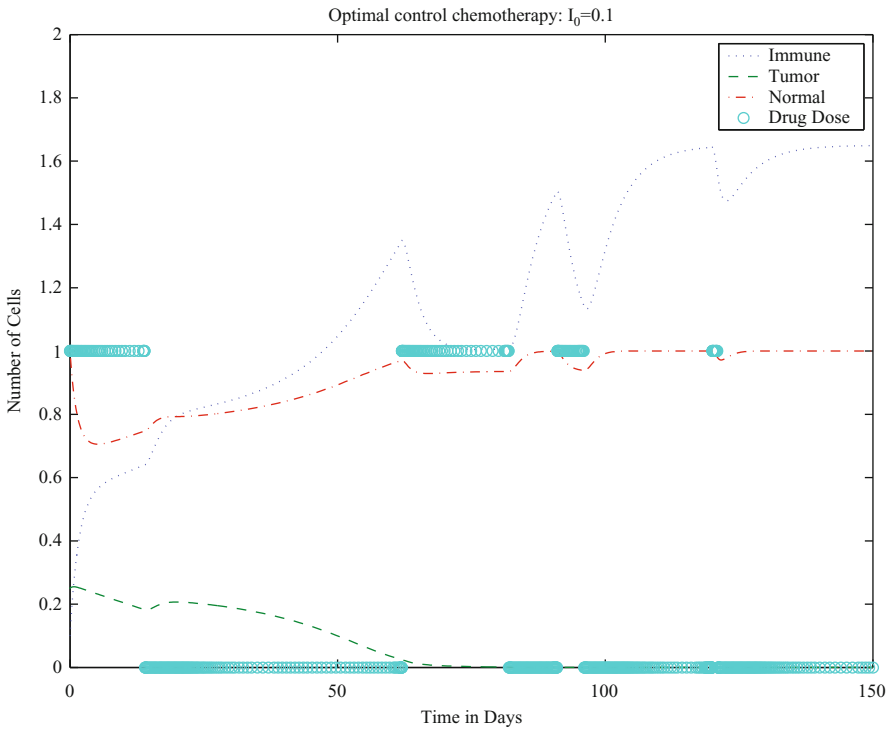
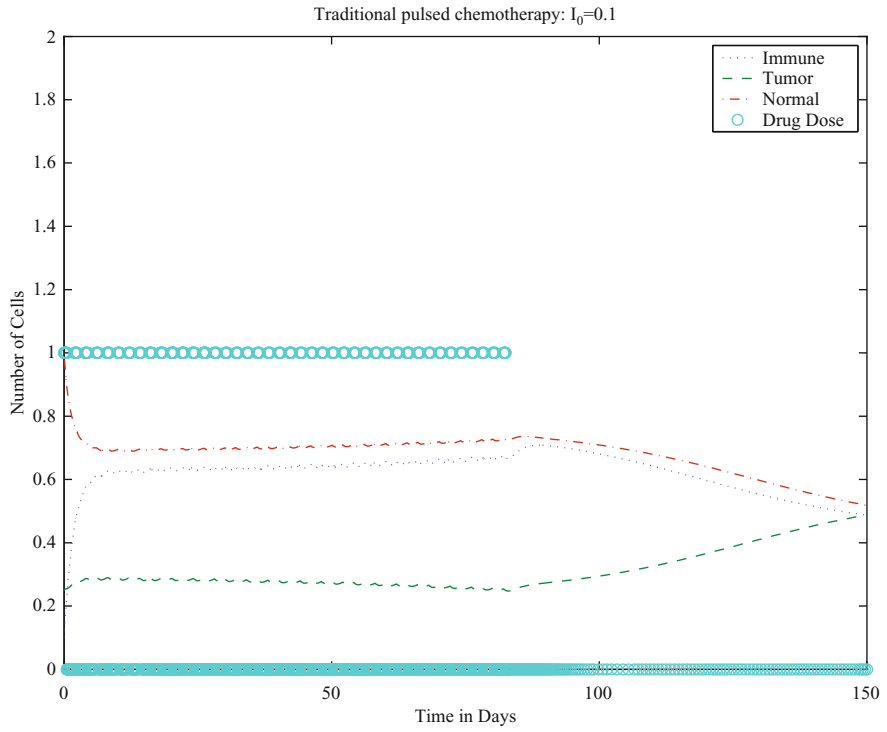


Fig. 5 (continued)

From there they are recruited to various lymph organs. When a nonself cell, or antigen, is encountered by a certain type of roving immune cells called *antigen-presenting* cells (APCs), they are engulfed, and pieces of the foreign cell are “presented” to the T-cells, activating them and causing them to proliferate into one population that can recognize and kill that particular type of foreign cell. Figure 6 gives a sketch of this process, where the antigen-presenting cell is a *macrophage*. Once the CTL is activated, it will seek out the specific antigen for which it is trained. Some activated CTLs will become memory cells, providing immunity for a second attack by the same foreign cells.

Note that other T-cells known as “helper T-cells” are also activated in this process, and these T-cells participate in the activation of the CTLs or “killer T-cells.” Helper T-cells will appear in our models later, in Sect. 4.1. Helper T-cells also activate B-cells, which are key players in the *humoral response*, that part of the immune response that is mediated by antibodies. Another important class of APCs is the *dendritic cells* (DCs), which are now being used in the development of cancer vaccines. These will be discussed in Sect. 4.2. In terms of the body’s fight against cancer, both NK cells and CTLs act like predators, but their methods of recognizing—and killing—their prey are different. As part of the innate immune system, natural killer cells are cytotoxic cells that are highly effective in lysing multiple (but specific) tumor cell lines [43]. Unlike cells of the specific immune system, which are drawn to a location due to the presence of antigen, the natural killer cells are constantly present guarding the body from infection and disease.

On the other hand, cytotoxic T lymphocytes are able either to lyse or to induce apoptosis in cells presenting *specific* antigens, such as tumor cells [43]. Unlike NK cells, CTLs are only able to recognize a specific antigen or tumor cell line. It is known, however, that these cells are able to destroy more than one tumor cell during their life cycle while a single natural killer cell generally kills very few [36]. After destroying the target cell, the CTLs move on in search of other antigen-presenting cells.

3.1 The dePillis–Radunskaya Law

In the fight against cancer, both the innate and the adaptive arms of the immune response are important. In fact, laboratory experiments show that without both NK cells and CTLs, tumors injected into mice will escape the immune surveillance



Fig. 5 *Left:* A patient with a relatively weak initial immune population ($I(0) = .1$ in normalized units) shows progressive disease after a series of pulsed chemotherapy treatments. The bolus treatments are simulated as injections at the maximum rate (normalized to $\max_v = 1$) for 12 h, repeated every 2 days for the course of the treatment. *Right:* A solution to the optimization problem given in Equation 3. The total amount of drug is the same in both the left (traditional treatment) and right (optimized treatment) simulations. The optimized treatment protocol is successful in eliminating the tumor

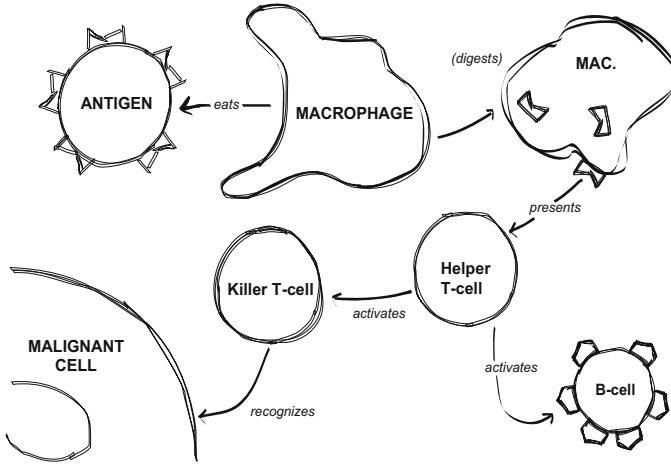


Fig. 6 A graphical representation of the activation of the adaptive immune response. A macrophage, a type of antigen-presenting cell (APC), recognizes a particular cell as “nonself” or antigen and engulfs it. The APC then presents bits of the engulfed, or “phagocytosed” cell to immature T-cells, which then begin to proliferate, activating other immune cells and, ultimately, the killer T-cells, or CTLs, and recognize and kill malignant cells of the same type as the initial antigen

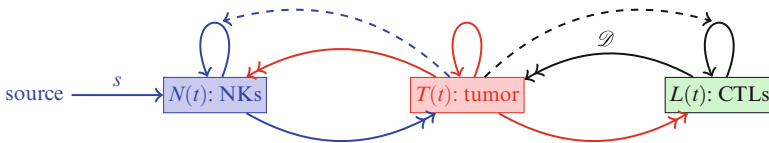


Fig. 7 Schematic of the model with two types of effector cells: natural killer cells (N), representing the innate immune response, and cytotoxic T lymphocytes (L), representing the adaptive immune response. As before, the solid lines represent direct interactions, with a single arrow-head denoting a cooperative interaction, and a double arrowhead denoting a competitive interaction. The dashed lines represent indirect interactions, where one population affects the *rate* of another interaction

(e.g., [18]). We therefore separate the effector cell population from the previous model into two subpopulations: the NK cells and the CTLs. Without the host cells, the model diagram becomes that shown in Fig. 7.

In developing the model, we assume again that the tumor grows logistically, that the NK cells, as part of the innate immunity, have a constant source, that immune cell proliferation is enhanced by the presence of the tumor, and that immune cells and tumor cells interact competitively. Furthermore, we know that the destruction of tumor cells by NK cells results in an increased uptake of antigen by antigen-presenting cells and, hence, an increase in the number of tumor-specific CTLs that are produced.

In the previous model given by System 1, competition between effector immune cells and tumor cells was represented by a mass action term of the form $-cIT$.

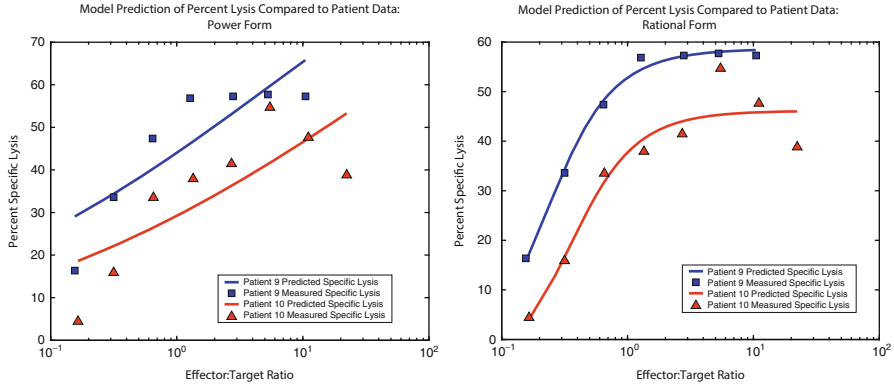


Fig. 8 *Left*: best fit kill rates using a power law for the per-cell kill rate by CTLs. *Right*: best fit kill rates using a ratio-dependent per-cell kill rate by CTLs. *Solid lines*: model simulations, **▲** and **■**: data for two patients from [23], Figure from [16].

This term reflects an assumption that the number of encounters between the two cell populations is proportional to the product of the two populations, i.e., that all immune–tumor cell pairs are equally likely to occur, and that each of these encounters has an equal chance of resulting in the death of the tumor cell. A more general assumption might be that it takes n immune cells to kill one tumor cell, in which case the competition term would take the form $-cI^nT$. However, in trying to fit experimental data to a power law for the kill rate, it became apparent that the kill rate by CTLs does not follow this function form. Figure 8 shows the best fit curves to data from [23] using both a power law and a saturating *ratio-dependent* kill rate of the form: $\mathcal{D} = -d \frac{(L/T)^\lambda}{k_{1/2} + (L/T)^\lambda} T$. The kill rate for NKs does, on the other hand, fit a power law quite well. This gives a mathematical distinction between the functional forms for the kill rates of the two types of effector cells and has become known as the *dePillis–Radunskaya Law*. See [16] for details.

In this model we continue to denote the tumor cell population by T . We now let N denote NK cells (rather than normal cells) and L denote the number of cytotoxic T lymphocytes. We include in our equations one more distinction between the innate and the adaptive response. Since the NK cells recognize antigen directly, the response term in the NK equation (Equation 6) depends explicitly on the tumor population: $\frac{gT^2}{h + T^2} N$. However, as depicted in the graphic in Fig. 6, CTLs are activated by a cascade of immune events, including antigen presentation by APCs and activation of helper T-cells. Since tumor cells must be lysed before the APCs can initiate the activation cascade, the response term in the CTL equation (Equation 7) depends on the kill rate of tumor cells which in turn is given by the sum of the ratio-dependent term from the dePillis–Radunskaya Law, \mathcal{D} , and the power law kill rate by NK cells, denoted by rNT .

To complete the model, we include a saturating response term. The model system is

$$\frac{dT}{dt} = aT(1 - bT) - cNT - \mathcal{D} \quad (5)$$

$$\frac{dN}{dt} = s - fN + \frac{gT^2}{h + T^2}N - pNT \quad (6)$$

$$\frac{dL}{dt} = -mL + \frac{j\mathcal{D}^2}{k + \mathcal{D}^2}L - qLT + rNT \quad (7)$$

where

$$\mathcal{D} = d \frac{\left(\frac{L}{T}\right)^\lambda}{k_{1/2} + \left(\frac{L}{T}\right)^\lambda} T, \quad (8)$$

With this model, we can now study the response of the system to variations in the two types of immune response. A sensitivity analysis shows that the final size of the tumor is most sensitive to the model parameter, d , which represents the maximum kill rate by CTLs. On the other hand, the size of the tumor after 40 days is affected by small changes in the parameter c , representing the strength of the kill rate by NK cells. This suggests that treatments should focus on increasing the number of CTLs, and enhancing their effectiveness and that the innate immune system cannot, by itself, control tumor growth.

The mechanisms that lead to the different kill rate laws are still unknown. It is likely that spatial effects are important, since CTLs are trained to “seek and destroy” specific antigens, while NK cells move randomly through the body. In the next section we introduce a spatial component into the model.

3.2 Adding a Spatial Component: Agent Based Models

One way to address questions about the effects of the spatial distribution of tumor and immune cells is to employ a hybrid cellular automata–partial differential equation modeling approach. The model we describe in this section is detailed in [39], and accounts for the spatiotemporal and stochastic interactions between individual tumor cells and populations of CD8+T (also known as CTLs) and NK cells while the tumor is in the pre-vascular stage.

We initialize the model with a cluster of tumor cells in a two-dimensional space of extra-cellular matrix (ECM). Nutrient diffuses from nearby blood vessels through the space to the tumor cells. In subsequent hybrid CA models [12, 22], we incorporated nutrient delivery through blood vessel sources interspersed throughout the computational domain. In the model presented here, we focus on the early pre-vascular stage, representing a small tumor burden, such as a postoperative remnant or a small satellite colony originating from a resected tumor.

As a result of the external nutrient supply, avascular tumors often develop into compact, nearly spherical structures. In these cases, the growing tumor generally develops three distinct layers—the proliferative rim, which is an outer shell of dividing cells that have direct access to nutrients that have diffused through the tissue; the quiescent layer, which is an inner layer of cells that have insufficient nutrient to allow them to divide, but enough to keep the cells alive; and a central core of necrotic cells that have died because nutrient concentrations are too low to maintain cell life. Our model simulations are able to produce a variety of tumor growth outcomes, including spherical and papillary (branchy) growth, stable and unstable oscillatory growth, proliferating and quiescent layers with a necrotic core, and lymphocyte-infiltrated growth. Lymphocyte infiltration is of particular interest given the experimental research that suggests improved survival rates for patients with intratumoral immune cells [60]. Infiltration of T-cells into the tumor mass can also lead to fibrosis and necrosis and subsequently reductions in tumor size [51, 54]. Numerical simulations of this model are in qualitative agreement with the experimental results demonstrated by, for example, Zhang et al. [60], Schmollinger et al. [51], and Soiffer et al. [54].

3.2.1 Hybrid PDE–CA Model Overview

Our model tumor grows on a two-dimensional square domain representing a patch of tissue that is supplied with nutrients by blood vessels that occupy the top and bottom boundaries, as shown in Fig. 9. The remainder of the space is partitioned into a regular grid in which the various cell types reside, and through which the nutrients diffuse. The grid is partitioned in such a way that each cellular automata grid

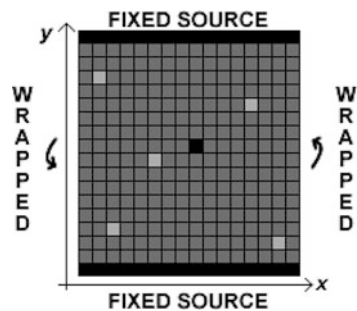


Fig. 9 Schematic of the cellular automata physical domain. The conditions imposed on the four boundaries are indicated. The solid bars (*top* and *bottom*) represent the capillaries while different cell types are shown filling the spaces in the grid

element corresponds in size with the actual biological cells of interest (10–20 μm [2, 38]). We simulate the time progression of the system using two main steps. First, we solve the reaction–diffusion equations for the nutrient species, then with dependence upon the new nutrient fields, the actions of the cells (such as migration and proliferation) are carried out. Each iteration therefore corresponds to the period of tumor cell division. That is, a period of approximately 0.5–10 days, depending on the cell type in question [33, 49].

We include two representative nutrient species (such as glucose and oxygen [28, 58])—the first nutrient, N , being a necessary component of the cell division processes, while the second, M , is essential for the cell to survive. The nutrients diffuse throughout the tissue space, and as they do so, they are consumed by the different cells that are resident in tissue.

The nondimensionalized reaction-diffusion equations for the two nutrients are

$$\frac{\partial N}{\partial t} = \nabla^2 N - \alpha(H + I)N - \lambda_N \alpha T N, \quad (9)$$

$$\frac{\partial M}{\partial t} = \nabla^2 M - \alpha(H + I)M - \lambda_M \alpha T M, \quad (10)$$

The cell species are identified by H for host cells (normal tissue), T for tumor cells, and I for immune cells. Also, α^1 is the normal rate of consumption of nutrient by host and immune cells, and $\lambda_N \geq 1$ and $\lambda_M \geq 1$ determine the excess consumption by the tumor cells of the two types of nutrient. We impose Dirichlet boundary conditions at the top and bottom of the domain, to represent the constant nutrient source coming from the blood vessel. The right and left edges of the domain are subject to periodic boundary conditions.

The evolution of the four cell populations proceeds according to a combination of probabilistic and direct rules. A summary of the action and interaction of the cell types follows.

Host cells: The host cells are considered passive: other than their consumption of nutrients, they allow tumor cells to freely divide and migrate.

Tumor cells: The tumor cells in this model can divide, die, or migrate in space. These processes depend upon nutrient levels, the relative abundance of cells of the immune system, and crowding due to the presence of other tumor cells. Tumor cells can die either because of insufficient nutrient levels or from active killing by immune cells.

Immune cells: CTL cells are recruited to the tumor location when natural killer cells lyse tumor cells or when CTLs and tumor cells interact. A single CTL is able to lyse more than one tumor cell [36], a feature reflected in our model.

¹In references [39] and [27], the authors choose to use α^2 instead of α , since α^2 reflects the squared form of the dimensional terms it replaces. For clarity, we simply use α here.

The immune cell actions in the model are summarized as follows: NK cells are generated at a rate to keep levels in constant proportion to the total number of cells in the domain, CD8+T cells are recruited to the tumor site, both NK and CD8+T cells can move through the computational domain, both NK and CD8+T cells can kill tumor cells, and both NK and CD8+T cells can die, either through deactivation by encounters with tumor cells or through apoptosis.

The cellular automata grid is initiated with a single cancer cell in the domain, along with the normal level, I_0 , of natural killer immune cells. The remainder of space available to cells is occupied by non-tumorous host cells.

Spatial Simulations: Tumor Growth, No Immune System

Simulations show that tumor morphology is dictated by relative consumption rates: lower consumption rates of nutrient by tumor cells lead to more compact tumors, while higher consumption rates lead to the papillary morphology.

Figure 10a shows the growth in the total number of tumor cells over time when the tumor is allowed to grow in the absence of any immune response, and tumor cell consumption rates are low relative to normal cells. Note the initially exponential growth phase (iteration 0 through 200), before a phase of linear growth (iteration 200 through 800). These growth characteristics mimic the growth rates of multicell spheroids described experimentally by Folkman [28] and mathematically by Greenspan [30].

Figure 10b displays the state of the system after 800 iterations. A roughly circular tumor with a radius of about 200 cells has developed in the center of the domain and is growing steadily toward the sources of the nutrient. Higher tumor cell densities are seen at the periphery of the tumor where it is surrounded by normal cells comprising

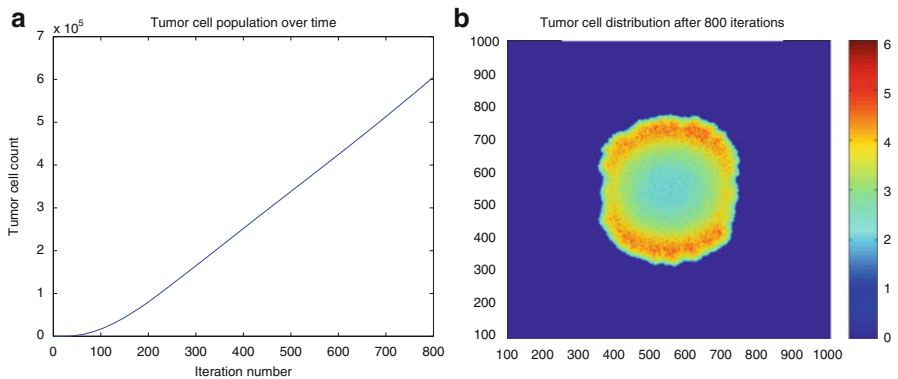


Fig. 10 Compact tumor growth in the absence of immune system interaction. Parameters: Domain size of 1000 elements $\approx 10\text{--}20$ mm, $t_{end} = 800$ cell division cycles, $\lambda_n = 50$, $\lambda_m = 25$, $\alpha = 1$, $I_0 = 0$. Note the beginning of a necrotic core in Fig. 10b. (a) Total tumor cell count over time (b) Final tumor cell distribution over the cellular automata grid

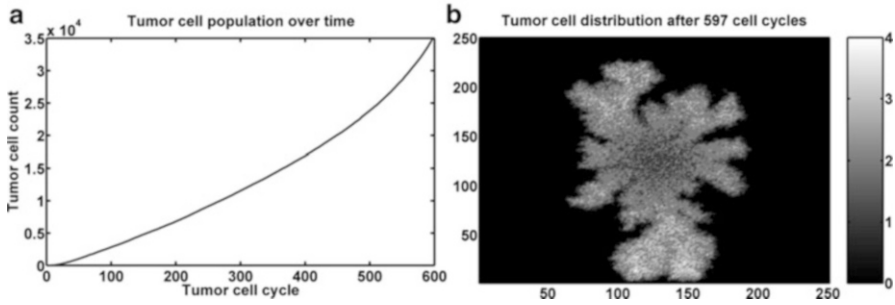


Fig. 11 An example of papillary tumor growth in the absence of immune system interaction. Parameters: Domain size of 250 elements ≈ 2.5 –4mm, $t_{end} = 597$ cell cycles, $\lambda_n = 100$, $\lambda_m = 10$, $\alpha = 2$, $I_0 = 0$. (a) Total tumor cell count over time (b) Final tumor cell distribution over the cellular automata grid

the host tissue. In the center of the tumor a necrotic core is beginning to form with some necrotic material already appearing. The tumor shown is growing in a domain that is approximately 10–20 mm square.

Figure 11 shows a tumor with relatively high nutrient consumption rates, a “gluttonous” tumor. Figure 11a shows the tumor cell count over time. We observe that the tumor is growing exponentially throughout the time considered without moving to a linear growth rate (as is seen in Fig. 10a). This may be due to the shape of the tumor and the lower requirements of the tumor cells for survival nutrient. Unlike the spherical tumors for which the cell-dense periphery limits the diffusion of nutrients to the tumor center, the papillary tumor grows out quickly from its origin and does not form a cell-dense border. Nutrients diffuse more readily throughout the domain, so a greater percentage of tumor cells is provided with the nutrients to both survive and divide.

Tumor Growth with the Immune System

We now add an immune cell to the simulation. In these experiments we use $I_0 = 0.01$ or 1% of the baseline value, consistent with biological levels measured in [38] and [8].

Figure 12 shows the effect on tumor (left figures) and immune (right figures) cell populations due to changes in CTL recruitment strength. All figures were produced with the same parameters as for Fig. 11, the papillary, “gluttonous,” tumor (except for the immune parameters). We see oscillatory population cell counts for both tumor and immune cells. Qualitatively similar results were observed for simulations using the compact tumor parameters (figures not shown).

Figures 12a–b show solutions for the highest level of CTL recruitment and very few oscillations are observed. While it appears in Fig. 12b that little has changed in the immune cell population, the important factor is the *location* of the immune cells. After detection of the tumor, the immune cells are attracted to the location of the tumor mass, thus aiding in its removal.

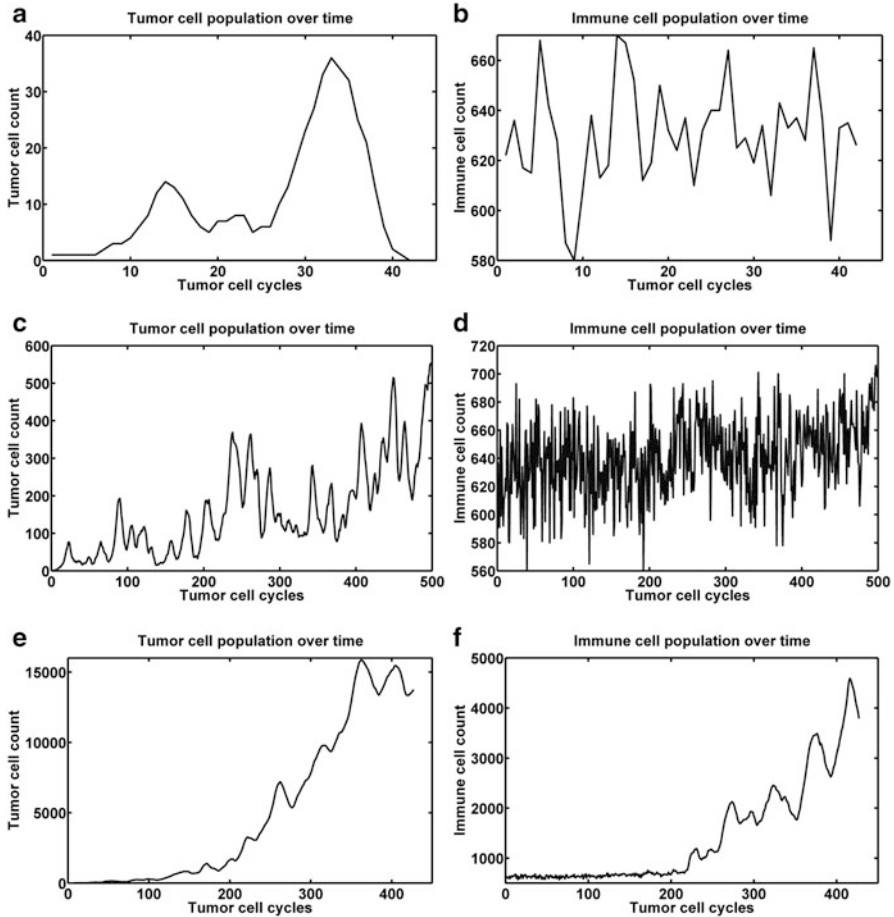


Fig. 12 The effect on tumor and immune cell distributions in compact tumors over time due to changes in CTL recruitment rates, which are inversely related to the parameter θ_L : a larger value of θ_L results in a lower recruitment rate. Parameters: Domain size of 250 elements $\approx 2.5\text{--}4\text{mm}$, $\lambda_n = 100$, $\lambda_m = 10$, $\alpha = 2$, $I_0 = 0.01$. (a) $\theta_L = 3$ (b) $\theta_L = 3$ (c) $\theta_L = 5$ (d) $\theta_L = 5$ (e) $\theta_L = 7$ (f) $\theta_L = 7$

For slightly weaker CTL recruitment, solutions are shown in Figs. 12c–d. The tumor cell population is oscillatory but trending upward. A number of simulations carried out with the same parameter set also exhibited this oscillatory behavior. Experimental evidence for such oscillatory behavior can be found in, for example, Kennedy [32] who studied chronic myelogenous leukemia, and Krikorian et al. [34] who looked at non-Hodgkin’s lymphoma.

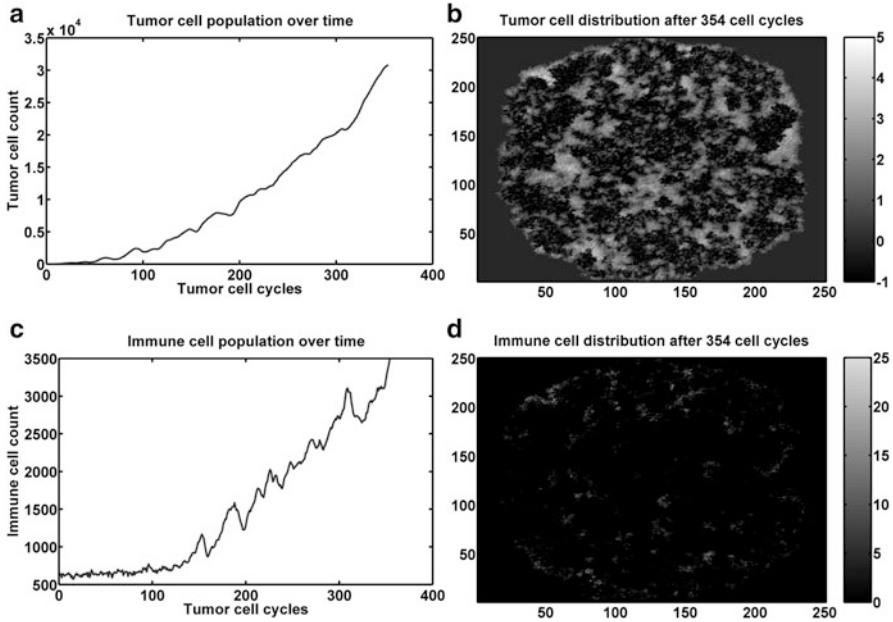


Fig. 13 Immune cell infiltration into a growing tumor. (a) and (b) show the tumor cell count over time and the final tumor cell distribution over the cellular automata grid, while the same outputs for total immune cells are shown in (c) and (d). Parameter values are domain size of 250 elements $\approx 2.5\text{--}4\text{mm}$, $t_{end} = 354$ cell division cycles, $\lambda_n = 50$, $\lambda_m = 25$, $\alpha = 1$, $I_0 = 1$. Computations were halted when the tumor cells reached the edge of the computational domain

In Figs. 12e–f the tumor and immune cell populations are shown for the case where CTL induction is very low. In this example, the tumor cell population is only slightly oscillatory. In other simulations using this parameter set, the low recruitment of T-cells leads to the tumor undergoing unstable, oscillatory growth.

Lymphocyte Infiltration

Studies have found the relationship between increased survival rates of cancer patients, tumor necrosis and fibrosis, and the presence of intratumoral T-cells, or infiltrated T lymphocytes [51, 54, 60]. The results shown in Fig. 13 simulate the infiltration of immune cells into a growing tumor. These are seen in the darker regions of Fig. 13b where tumor cell necrosis has occurred and in the lighter regions of Fig. 13d where the immune cell numbers are highest. These solution plots are similar to experimental results shown by Schmollinger et al. [51], Soiffer et al. [54],

and Zhang et al. [60] where strings of immune cells are moving into the tumor, surrounding individual cells and causing tumor cell necrosis. In Sect. 4.2 we test the effect of injecting immune cells directly into the tumor.

4 Modeling Immunotherapies

We have seen that an individual's immune response to a cancer tumor is a crucial factor in determining the progression of the disease. Cancer immunotherapy is a treatment for cancer that attempts to enhance this immune response. There are a range of different types of immunotherapies, and they can be generally classified into cytokine therapy, cellular transfer, antibody therapy, and vaccines. Newer cytokine treatments called "checkpoint blockades" target specific receptors on T-cells that block or slow their response. These immunotherapy modalities can be broad, targeting the immune system as a whole, or they can be specific, targeting the immune response to a specific cell type. Cancer vaccines are specific: they are intended to enhance the adaptive immune response either by making the tumor-specific immune cells more abundant or more effective or by making the tumor cells more immunogenic, i.e., more recognizable by the cells in the adaptive arm of the immune system. One type of vaccine that has shown some promise in melanoma is a *peptide* vaccine. Peptides are proteins found on cells, and a peptide vaccine targets proteins, or antigens, that are found only on the tumor cells. The idea is to isolate these peptides and to administer them in large doses to the patient in order to stimulate an immune response. The antigen-presenting cells will recognize the peptide, and will initiate the cascade of events roughly depicted in Fig. 6 that will result in the production of tumor-specific CTLs and, ultimately, the destruction of tumor cells. The difficulty is in identifying these peptides, since they must be specific to the patient's own tumor cells but not found, or rarely found, on normal cells. Promising peptides have been found for melanoma and breast cancer [3]. A big advantage that peptide vaccines have over other treatments are their low toxicity, since they promote an immune response targeted only at the tumor cells.

The big questions in the administration of cancer vaccines are: How much? How often? Where? Mathematical models can help suggest answers to these questions. In this section we model three types of cancer immunotherapy and indicate how the model results can inform clinical practice.

4.1 *The Kinetics of the Immune Response to Peptide Vaccines: Dose Scheduling*

The effectiveness of a peptide vaccine could be measured by the size of the immune response. In the laboratory, the kinetics of this immune response can be measured

in mice by injecting them with vaccine and then counting the number of antigen-specific T-cells that result. We would like to know what dosing schedule maximizes this response. The proliferation of T-cells occurs in the lymph organs, so we will model the T-cell populations in the main lymph organ of the mouse: the spleen. We will introduce the helper T-cells into the model, since they are important players in the speed and magnitude of the response.

Once the injected peptides are taken up by antigen-presenting cells, these APCs travel to the spleen where they activate naive T-cells. This activation process takes time to initiate, and we denote this activation time, or *synaptic connection time*, by τ_N . Once activated, the T-cells then begin to proliferate rapidly. After this expansion phase, the activation process is shut down, and the activated T-cells move out of the spleen to find the tumor, become memory T-cells, ready to be activated when the system is next challenged with the same antigen, or become apoptotic, dying off quickly. To describe this process and to capture the dynamics of the T-cell populations when the vaccine is given in repeated doses, the T-cell populations will be divided into five subpopulations: naive, proliferating, active (able to seek and destroy tumor cells), memory cells, and apoptotic cells. The graphic in Fig. 14 shows the five stages, with a dendritic cell as the APC. Note that two synaptic connection times are shown by the dashed lines: τ_N is the time required for activation of the naive T-cells, and τ_M is the activation time required for memory T-cells. Since the memory cells are already trained to recognize the specific antigen, they can be activated more quickly, so that $\tau_M < \tau_N$.

To model the immune activation process mathematically, we use a system of *delay-differential* equations. There is an equation for each state of each cell type

Five stages for each type of T-cell: $CD8^+$ (killer cells) and $CD4^+$ (helper cells)

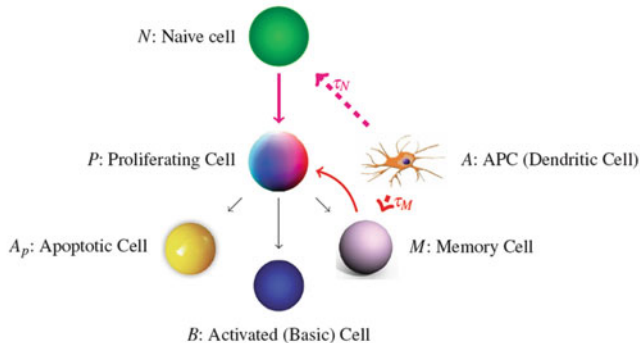


Fig. 14 Schematic diagram representing the model of the T-cell response to antigen. The response takes place in a lymph organ (e.g., the spleen) and is initiated by an antigen-presenting cell (APC), here represented by a dendritic cell (DC). The T-cells can be in one of five stages, represented here by balls. *Dashed arrows* represent the delays in the model, which show up in the rate of proliferation in response to the presence of the APCs. The two types of T-cells (killer cells and helper cells) respond with different delays. The basic, active immune cells (labeled *B*) leave the lymph compartment to seek out the antigen

and one for the APCs. This gives a system of 11 equations, with four delays: two synaptic connection times for each of the cell types. For each of the two cell types (killer cells: $CD8^+$ and helper cells: $CD4^+$) we have the five equations 12–16:

APCs arrive from blood and activate naive and memory cells

for each type, $CD8^+$ and $CD4^+$:

$$\frac{dA}{dt} = \mu_{BS} D_B - \delta_A A(t) - d_{AT} A(t) (N(t) + M(t) + P(t)) \quad (11)$$

After synaptic connection times, τ_N and τ_M , activated naive and memory cells begin to proliferate:

$$\frac{dN}{dt} = s_N - d_N N(t) \quad (12)$$

Expansion phase: after contact with antigen, cells reproduce rapidly:

$$\begin{aligned} \frac{dP}{dt} = & g_1 A(t - \tau_N) N(t - \tau_N) + \lambda A(t - \tau_M) M(t - \tau_M) + \rho \frac{A(t - \tau) P(t - \tau)}{\theta + A(t - \tau)} \\ & - \delta_P P(t) - \frac{1}{T} P(t) \end{aligned} \quad (13)$$

Contraction phase: cells become memory (M), die quickly, or go to the blood (B):

$$\frac{dAp}{dt} = \frac{1}{T} P(t) - (r + \alpha + \delta_{Ap}) Ap(t) - \left(\mu_{SB}^* + \frac{\Delta\mu}{1 + A(t)/\theta_{shut}} \right) Ap(t) \quad (14)$$

$$\frac{dB}{dt} = \left(\mu_{SB}^* + \frac{\Delta\mu}{1 + A(t)/\theta_{shut}} \right) Ap(t) \quad (15)$$

Memory cells remain after antigen is cleared, with a homeostatic term:

$$\frac{dM}{dt} = rAp(t) + pM(t) \left(1 - \frac{M(t)}{k} \right) \quad (16)$$

Parameters were estimated from the literature and fit to experimental data as described in [47]. All parameter values can be found there. Model simulations show that, after a bolus infusion of peptide vaccine, the CTL population peaks at approximately 6.9 days and the helper T-cell population peaks lower and later, at approximately 8.12 days. See Fig. 15 for a sample simulation. Based on this simulation (which is fit to experimental data with essential, the same kinetic profiles), one might think that administering a second dose of vaccine at approximately Day 6 would result in a high level of T-cells.

To give a more informed answer to the question of when to administer successive doses of the vaccine, we can again formulate and solve an optimization problem, as we did in Sect. 2.1. As in that optimization problem, our goal is to choose the input function that maximizes a desired output. Again, the input function is the dose of the vaccine that produces the source term $D_B(t)$ for the antigen-presenting

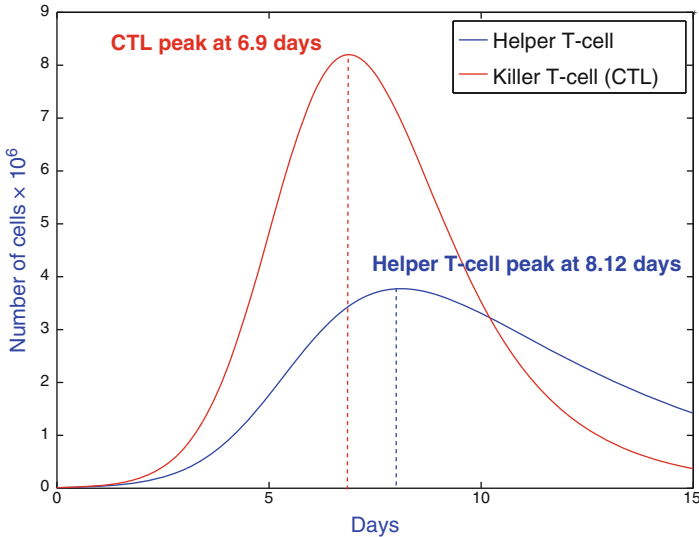


Fig. 15 Model System 11 through 16 simulated for both the CTL and the helper T-cell populations in the spleen. One bolus injection of a peptide antigen was given at time $t = 0$. Total population levels are shown (the sum of naive, proliferating, apoptotic, basic, and memory). The CTL levels peak higher and earlier than the helper T-cell levels. For parameter values and other details see [47]

cells, shown in Equation 11. However, because this system has more equations and four delays, it is too complicated to solve by analytical or direct collocation methods. Instead, we can employ a heuristic optimization scheme to find candidates for optimal solutions. As an example, many runs of a genetic algorithm applied to the system with three different fitness functions yielded the results shown in Fig. 16. In practice, thousands of runs are performed, and those with the highest valued fitness functions are candidates for optimal dosing schedules. In this case, the genetic algorithm suggests that the second dose be given at Day 3—earlier than our first guess of Day 6 based on the kinetics of the response to the first dose. This hypothesis has since been tested in the laboratory on mice confirming the results of the optimization problem [47]. Current vaccine protocols are rigidly set, often at longer intervals than suggested here [9]. We hope that this model and its refinements can serve as a guide for the design of treatment strategies in the future. One possible extension is discussed in Sect. 4.2.

4.2 Dendritic Cell Vaccines

Peptide vaccines, discussed in Sect. 4.1, require the identification of peptides that are expressed on the tumor cells of all patients with that type of cancer (e.g., melanoma), but that are *not* found on normal cells. One of the limitations of this

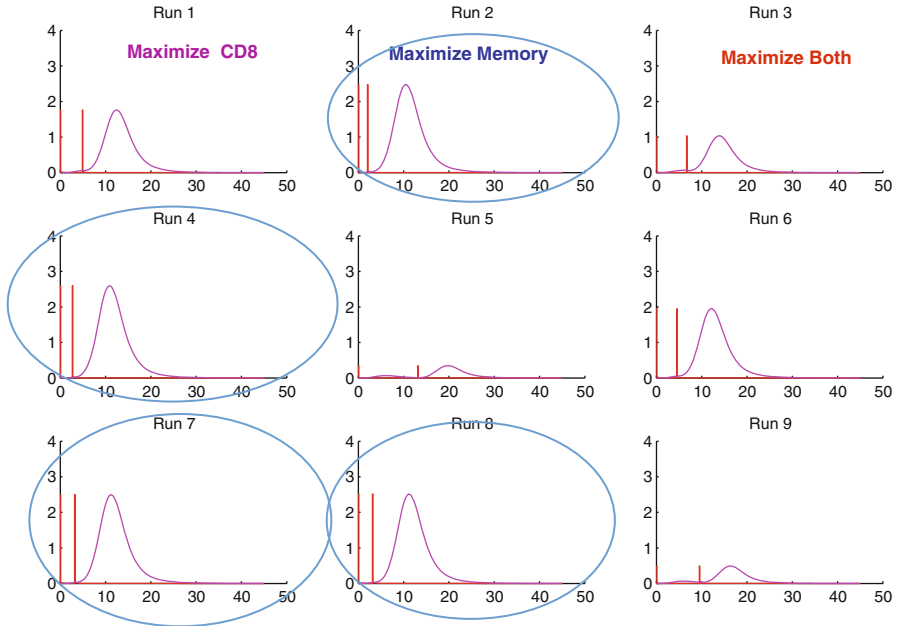


Fig. 16 The solutions with the highest fitness level for 9 different runs of the genetic algorithm. In the first column, the fitness function was the number of $CD8^+$ or CTLs. In the second column, the fitness function was the number of memory T-cells. In the third column, the fitness function was a linear combination of both the CTL population and the memory cell population. Considering all three columns, the runs that yielded the highest fitness values show that the second peptide dose is given at approximately Day 3, (circled runs). Red bars indicate the administration times for the two bolus injections of vaccine

type of therapy is that tumor-specific antigens are rare. Another approach is to use vaccines that are developed from the patient’s own immune cells, known as “autologous” vaccines. Dendritic cell vaccines are a type of *immune cell-based* vaccine, where immune cells (in this case, dendritic cells, but other APCs are also involved) are removed from the patient, activated by tumor-associated antigen and immune-activating cytokines (such as granulocytes-macrophage colony-stimulating factor, GM-CSF), and cultivated. This expanded colony of activated DCs is then injected into the patient, with the goal of stimulating the tumor-specific immune response modeled in Sect. 4.1. One advantage that autologous DC vaccines have over other, more systemic, treatments is that they have very few toxic side effects: the patient is receiving immune cells of their own making, activated to attack only their own tumor cells. The first such vaccine to be approved by the FDA began to be tested in 2010, with encouraging but not definitive results [9]. During the clinical trial, a fixed dosing regimen was rigidly imposed for all patients: three rounds of vaccines were given every two weeks. Given the sensitivity of the immune kinetics to the timing of the boosting doses, it is likely that outcomes could be improved



Fig. 17 Schematic representation of the DC trafficking model. There are three compartments: spleen, blood and tumor. Different cell populations exist in each department, some of which move from one compartment to another. *Arrows* indicate the flow from one compartment to another, with labels showing which cell populations actually move

by varying the dose and timings. Another variable is the location of the injection: should the vaccine be injected into the tumor site, where the initiation of the immune response normally occurs, or should it be injected into the bloodstream, which is easier and allows the new immune cells to go wherever they are most needed?

In order to answer the three questions: How much? How often? and Where?—a tumor cell population must be added to the model, and the trafficking of the immune cells between the lymph organs and the tumor must be described. We do this in the simplest way possible, by adding a tumor compartment and a blood compartment to the spleen compartment described in Equations 11–16. To reduce the complexity of the model, we focus on the killer T-cells and omit for the time being the helper T-cells. Tumor–immune interactions in the tumor compartment are described by the dePillis–Radunskaya Law, since we are looking at the adaptive response. A schematic is given in Fig. 17.

The dynamics of the trafficking of the immune cells from one compartment to another are complex, with experimentally observed “trapping” effects in both the spleen and the tumor compartments. This results in some rather complicated expressions for the influx and outflow rates in the spleen and tumor compartments: details can be found in [48]. The full set of equations is

Blood compartment:

$$\frac{d}{dt} D_{blood} = -\mu_B D_{blood} + \mu_{TB} D_{tumor} + v_{blood}(t) \quad (17)$$

$$\frac{d}{dt} E_{blood}^a = \mu_{SB}(D_{spleen}) E_{spleen}^a - \mu_{BB} E_{blood}^a \quad (18)$$

$$\frac{d}{dt} E_{blood}^m = \mu_{SB}(D_{spleen}) E_{spleen}^m - \mu_{BB} E_{blood}^m \quad (19)$$

Spleen compartment:

$$\frac{d}{dt} D_{spleen} = D_{\max} \left(1 - e^{\left(\frac{-\mu_{BS} D_{blood}}{\theta_{shut}} \right)} \right) - a_D D_{spleen} - b_{DE} E_{spleen}^a D_{spleen} \quad (20)$$

$$\begin{aligned} \frac{d}{dt} E_{spleen}^a = & \mu_{BSE} E_{blood}^a - \mu_{SB}(D_{spleen}) E_{spleen}^a + b_a D_{spleen} E_{spleen}^m \\ & + a_{EaS} (DC_{on} E_{naive} - E_{spleen}^a) - r_{am} E_{spleen}^a \\ & + b_p \frac{D_{spleen}(t - \tau_D) E_{spleen}^a(t - \tau_D)}{\theta_D + D_{spleen}(t - \tau_D)} \end{aligned} \quad (21)$$

$$\begin{aligned} \frac{d}{dt} E_{spleen}^m = & r_{am} E_{spleen}^a - (a_{Em} + b_a D_{spleen} + \mu_{SB}(D_{spleen})) E_{spleen}^m \\ & + \mu_{BSE} E_{blood}^m. \end{aligned} \quad (22)$$

Tumor compartment:

$$\frac{d}{dt} E_{tumor}^a = \mu_{BTE}(T) E_{blood}^a - a_{EaT} E_{tumor}^a - c E_{tumor}^a T \quad (23)$$

$$\frac{d}{dt} T = rT \left(1 - \frac{T}{k} \right) - \mathcal{D} \quad (24)$$

$$\frac{d}{dt} D_{tumor} = \frac{mT}{q + T} - (\mu_{TB} + a_D) D_{tumor} + v_{tumor}(t) \quad (25)$$

The “trapping” term which describes the observed phenomenon of activated CTLs being held back in the spleen in the presence of DCs is

$$\begin{aligned} \mu_{SB}(D_{spleen}) = & \mu_{SB}^* + \frac{\Delta\mu}{1 + \frac{D_{spleen}}{\theta_{shut}}}, \\ \Delta\mu = & \mu_{SB}^{Normal} - \mu_{SB}^*. \end{aligned}$$

The functions $v_{blood}(t)$ and $v_{tumor}(t)$ allow us to model injections of DCs into the blood and tumor, respectively. In the tumor compartment, the response rate of the CTLs due to the presence of the tumor has a saturation term

$$\mu_{BTE}(T) = \mu_{BB}(T/(\alpha + T)).$$

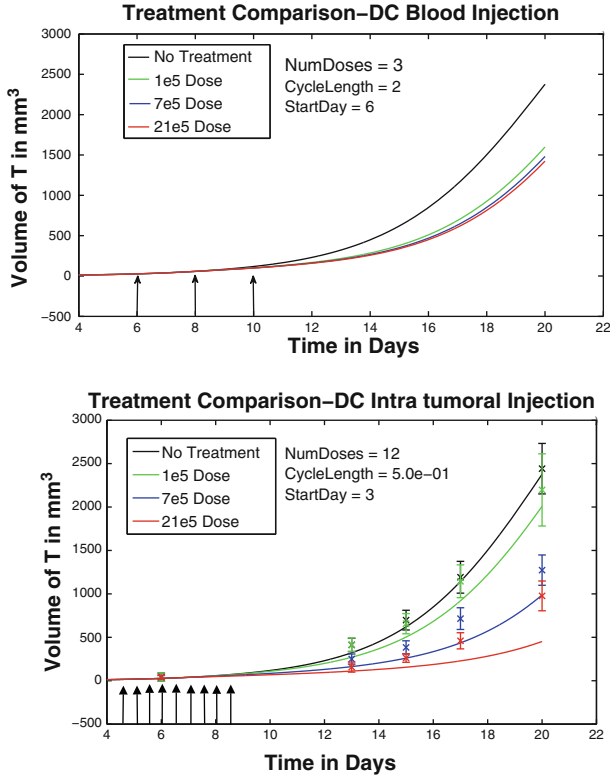


Fig. 18 Comparison of two dosing schedules and injection location. Vaccination treatment starts on Day 6, is injected into the blood, and is given in three doses every two days (*left*), compared to a vaccination regime starting on Day 3, injected directly into the tumor, and given in 12 doses, twice a day (*right*). Times of vaccine doses are shown by arrows (the first two doses are not shown on the *right*)

The ratio-dependent kill rate, \mathcal{D} , in Equation 24 is the one described in Sect. 3.1, Equation 8. Note that the effector T-cells denoted by E_{tumor}^a in this model play the role of the CTLs, denoted by L in Equation 8.

This model allows us to experiment with different dosing, timing, and location strategies in order to determine optimal outcomes. Two scenarios are compared in Fig. 18 to give an idea of the flexibility of the model. From these experiments (and others not shown) we can hypothesize that, in the context of DC vaccines, 1) vaccines administered into the blood stream are more effective than those injected directly into the tumor and 2) fractionated dosing schedules are more effective. These hypotheses could be tested in a laboratory or clinical setting, the model refined, and new hypotheses formed. See [48] for more details about the model, parameter settings, and the results of other simulation experiments. Clinical trials of cancer vaccines have had mixed results, where some patients respond well, and

others do not [3, 45]. In addition to providing insights into improving treatment protocols, mathematical models can also suggest ways to identify patients who will respond to a particular treatment. Once the model is formulated a sensitivity analysis can indicate which model parameters have the most effect on specific outcomes. A sensitivity analysis using Latin hypercube sampling was performed on this model, indicating that the immune response parameter, d , appearing in the \mathcal{D} term (Equations 24 and 8) has a large impact on the progression of the tumor, and that this effect is enhanced when a patient receives a DC vaccine. A comparison of tumor growth, with and without DC vaccine therapy, with various values of d , is shown in Fig. 19.

4.3 Monoclonal Antibody Therapy

In addition to peptide and immune cell vaccines, antibody-mediated therapy has been used either alone or in conjunction with other treatments. In this next model, we capture the dynamics of colorectal cancer growth and its response to monoclonal antibody (mAb) therapy in combination with chemotherapy. We show how the model can be used to simulate clinical trials, a safe and efficient way to lower expenses and speed up the process of treatment design. The work described in this section is extracted from [13], in which further details can be found. Monoclonal antibodies are manufactured to bind to specific proteins. Various protein targets can be used, but epithelial growth factor receptor (EGFR) is a common and useful choice. Circulating epithelial growth factor (EGF) binds to the EGFR and signals a cell proliferation cascade. Many cancerous cells, including colorectal cancer cells, have an EGFR-upregulating mutation, thought to be partly responsible for the high proliferation rate of tumor cells [17, 29, 40, 53]. Monoclonal antibodies can block the EGFR, potentially preventing further tumor cell proliferation.

There are three main pathways for mAb-induced tumor death (see Fig. 20): interactions between mAbs, NK cells, and tumor cells; interactions between mAbs, chemotherapy, and tumor cells; and interactions only between mAbs and tumor cells, resulting in growth rate reduction, complement activation, and possibly other mechanisms for tumor death. In this model, we have chosen to include the following components:

- Cell populations
 - $T(t)$: the total tumor cell population;
 - $N(t)$: the concentration of NK cells per liter of blood (cells/L);
 - $L(t)$: the concentration of CTLs per liter of blood (cells/L);
 - $C(t)$: the concentration of other lymphocytes (cells/L).
- Medications (chemotherapy, cytokines, and monoclonal antibodies); and treatments:
 - $M(t)$: the concentration of chemotherapy per liter of blood (mg/L);
 - $I(t)$: the concentration of interleukin per liter of blood (IU/L);

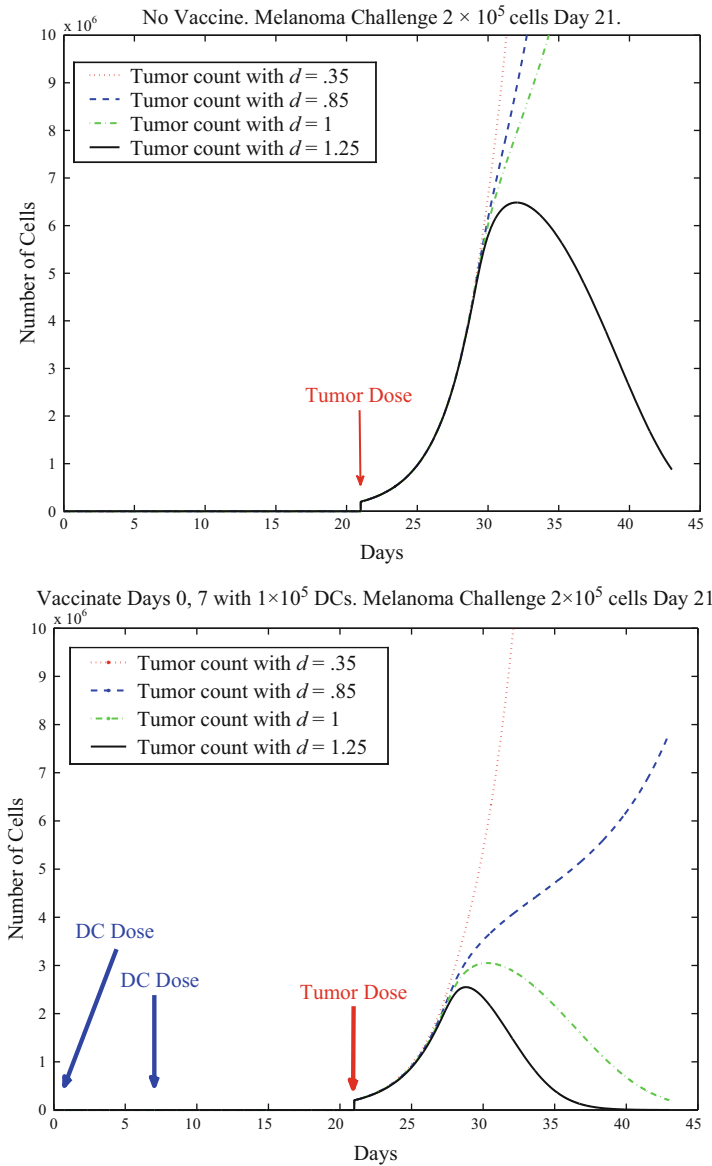


Fig. 19 Prophylactic vaccination and the effect of varying immune response parameter d . *Left*, no vaccine. *Right*, vaccinate with DC treatments on Days 0 and 7 with 1×10^5 DCs per dose. Tumor challenge on Day 21, with 2×10^5 tumor cells. Dosing follows the experiment described in [46]. With $d = 1$, the tumor is controlled as a result of vaccination; with $d = 1.25$ the tumor is controlled independent of vaccination

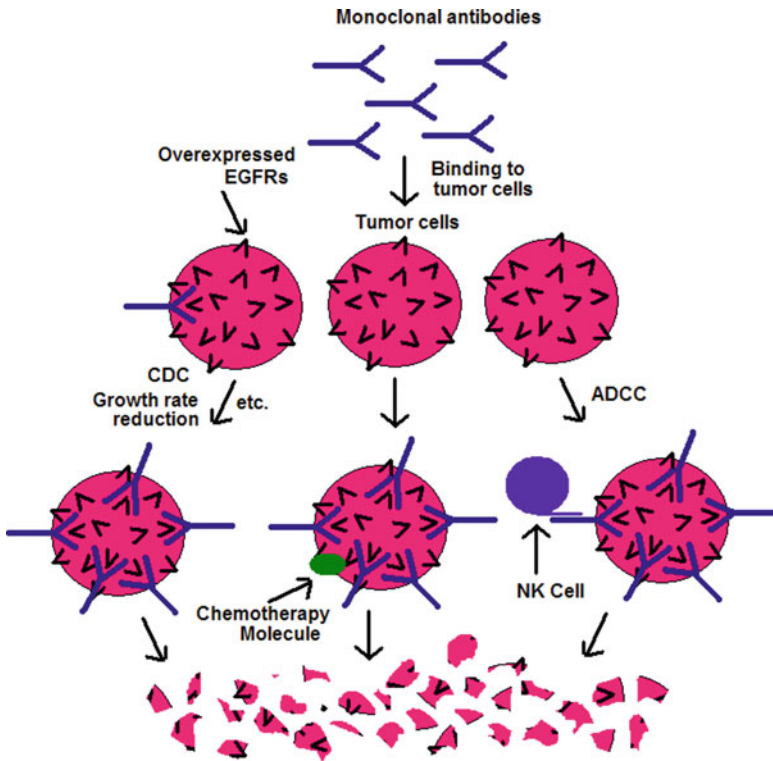


Fig. 20 Three methods of mAb-induced tumor cell death are represented in this model. If an NK cell is present then the cell can undergo ADCC, if a chemotherapy molecule is present then the cell will increase death from the chemotherapy drug, and otherwise, the MAB molecule will cause tumor cell death on its own, through a variety of mechanisms

- $A(t)$: the concentration of monoclonal antibodies per liter of blood (mg/L);
- $v_M(t)$: the amount of irinotecan injected per day per liter of blood (mg/L-day);
- $v_A(t)$: the amount of monoclonal antibodies injected per day per liter of blood (mg/L-day).

Equations (26)–(32) are the system of equations for this model.

$$\begin{aligned}
 \frac{dT}{dt} = & aT(1 - bT) - (c + \xi \frac{A}{h_1 + A})NT - \mathcal{D} \\
 & - (K_T + K_{AT}A)(1 - e^{-\delta_T M})T - \psi AT
 \end{aligned} \tag{26}$$

(continued)

$$\begin{aligned} \frac{dN}{dt} = & eC - fN - \left(p + p_A \frac{A}{h_1 + A}\right)NT + \frac{p_N NI}{g_N + I} \\ & - K_N(1 - e^{-\delta_N M})N \end{aligned} \quad (27)$$

$$\begin{aligned} \frac{dL}{dt} = & \frac{\theta mL}{\theta + I} + j \frac{T}{k + T}L - qLT + (r_1 N + r_2 C)T - \frac{uL^2 CI}{\kappa + I} \\ & - K_L(1 - e^{-\delta_L M})L + \frac{p_I LI}{g_I + I} \end{aligned} \quad (28)$$

$$\frac{dC}{dt} = \alpha - \beta C - K_C(1 - e^{-\delta_C M})C \quad (29)$$

$$\frac{dM}{dt} = -\gamma M + v_M(t) \quad (30)$$

$$\frac{dI}{dt} = -\mu_I I + \phi C + \frac{\omega LI}{\xi + I} \quad (31)$$

$$\frac{dA}{dt} = -\eta A - \lambda T \frac{A}{h_2 + A} + v_A(t) \quad (32)$$

where the immune response term \mathcal{D} has the familiar form given in Equation 8. The specific treatments that we will explore are the chemotherapeutic drug irinotecan (CPT11), and mAb treatments cetuximab or panitumumab.

4.3.1 Clinical Trial Simulations for mAb Therapy and Chemotherapy

We used the model to explore expected responses to treatment at a population level. In particular, we simulated response to treatment for a group of individuals with a range of immune “strengths.” In order to simulate a group of patients having differing immune strengths, we varied the parameters d , λ , and $k_{1/2}$ in Equation 8 for each individual simulated. To reflect the heterogeneity in response to treatment, we also varied the parameters K_T and ψ .

In our clinical trial simulations, we assume that individuals have slightly compromised immune systems after already having been through other immunodepleting therapies, reflected in a relatively low value of the initial immune cell population. Simulated treatments were administered to each patient, represented by $v_M(t)$ and $v_A(t)$ in model equations (30) and (32). We ran simulations over the set of 64 virtual patients, each identified by a parameter set with different values of the parameters d , $k_{1/2}$, λ , K_T , and ψ , and recorded final tumor size and lymphocyte counts. Lymphocyte count was used as a marker for patient health—if

the lymphocyte count dropped low enough for the patient to be considered grade 4 leukopenic, the treatment was considered to be too harsh and not useful.

In order to validate and calibrate our model, we compare the results of the simulated trials to those reported in [11, 17, 29, 31, 37]. Note that the published clinical trial results for cetuximab and panitumumab that we used for comparison reported results as “Response” or “No Response” almost exclusively, so our simulation outcomes reflect this categorization. We carried out monotherapy clinical trial simulations for each of the three drugs used in our model. Monotherapy results can be seen in Fig. 21. Our simulated response to irinotecan was purposefully lower than the clinical trial response, since we assume that our population of patients who may be treated with mAb therapy should be less responsive to chemotherapy than the general population. Our simulated responses to cetuximab and panitumumab were a very close match to the clinical trial outcomes. We also simulated combination therapies, using either irinotecan with cetuximab or irinotecan with panitumumab. These simulations used the common treatments for each drug and gave the two treatments simultaneously. Again, our simulations match the reported clinical trial results fairly closely (see Fig. 22).

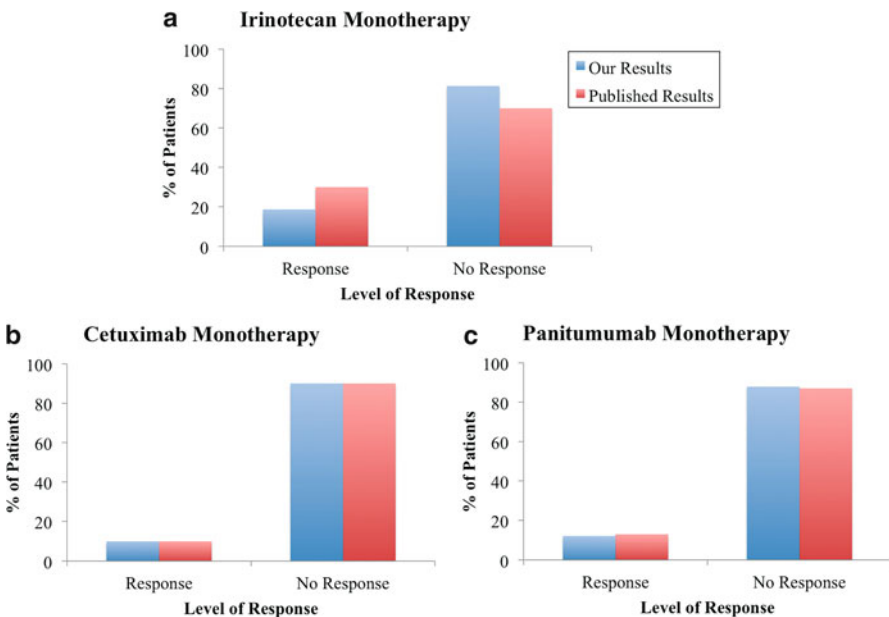
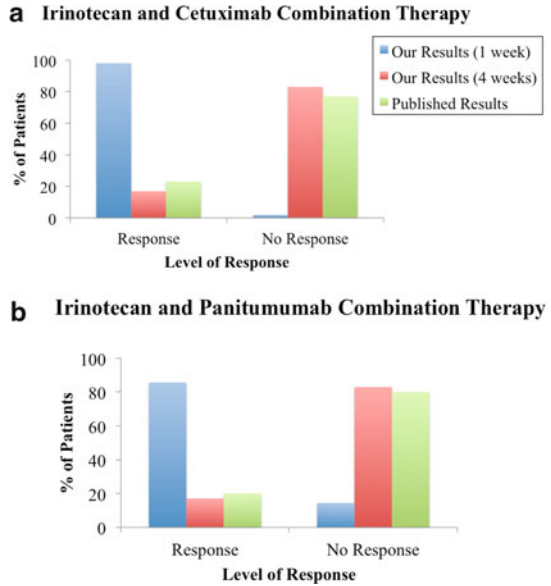


Fig. 21 Our clinical trial simulations compared to reported clinical trial results for irinotecan monotherapy (A), cetuximab monotherapy (B), and panitumumab monotherapy(C). Our simulation results (*left* bars) closely match published results (*right* bars) for both cetuximab and panitumumab monotherapies. For irinotecan monotherapies, the reduced response seen in our simulations is intended, since the patients receiving mAb therapy are often not as responsive as most patients to other treatments

Fig. 22 Our clinical trial simulations compared to reported clinical trial results for irinotecan and cetuximab combination therapy (A) and irinotecan and panitumumab combination therapy (B). When simulation results are measured four weeks post-treatment, our results are very similar to published results



5 Concluding Remarks

In this chapter we have presented brief glimpses of several mathematical models of the interaction between the immune system and cancer tumors. These models can be used to understand the dynamics of the tumor–immune interaction, predict the progression of the disease, and design effective treatment strategies that minimize toxicity. To date, the mathematical models have suggested the advantage of altering traditional protocols, for example, fractionated (or “metronomic”) dosing seems to be more effective—and less toxic—than bolus doses. They have helped provide functional forms for cell interactions that can differentiate between the two arms of the immune response. They can help us understand the effects of combined therapies, allowing researchers to move more swiftly and safely from “bench to clinic.” Finally, the analysis of these mathematical models, combined with advances in technology that provide us with an increased ability to accurately and noninvasively measure physiological parameters, can lead to the design of patient-specific treatment regimens. Once calibrated to a particular patient, mathematical models can be used to suggest treatment combinations and dosing protocols that are personally optimized.

Much work remains to be done—we hope that the few ideas presented here will motivate mathematicians, clinicians, systems biologists, programmers, and laboratory researchers to continue to collaborate with the goal of understanding and fighting the many diseases known as “cancer”.

Acronyms. NK, natural killer Cell; CTL, cytotoxic T lymphocyte, or Killer T-cell, also known as a CD8⁺ or cytotoxic T-cell because it has a glycoprotein called

CD8 on its surface; CD4⁺, helper T-cell, expresses the CD4 protein on its surface; ECM, extracellular matrix; IL2, interleukin 2, an immune-stimulating cytokine; APC, antigen-presenting cell; DC, dendritic cell, a type of antigen-presenting cell; EGF, endothelial growth factor; EGFR: endothelial growth factor receptor; mAb, monoclonal antibody

Acknowledgment Earlier, more detailed versions of much of the material in this chapter was published in [13–16,39,47,48]. A. Radunskaya was partially supported by NSF grant DMS-1016136.

References

1. J.A., Adam, N. Bellomo, *A Survey of Models for Tumor Immune Systems Dynamics* (Springer, Newyork, 1997)
2. T. Alarcon, H. Byrne, P. Maini, A cellular automaton model for tumour growth in inhomogeneous environment. *J. Theor. Biol.* **225**, 257–274 (2003)
3. G. Alatrash, H. Jakher, P.D. Stafford, E.A. Mittendorf, Cancer immunotherapies, their safety and toxicity. *Expert Opin. Drug Saf.* **12**, 631–645 (2013)
4. N. Bellomo, A. Bellouquid, M. Delitala, Mathematical topics on the modelling complex multicellular systems and tumor immune cells competition. *Math. Models Methods Appl. Sci.* **14**(11), 1683–1733 (2004)
5. N. Bellomo, L. Preziosi, Modelling and mathematical problems related to tumor evolution and its interaction with the immune system. *Math. Comput. Model.* **32**(3), 413–452 (2000)
6. A. Cappuccio, M. Elishmereni, Z. Agur, Cancer immunotherapy by interleukin-21: potential treatment strategies evaluated in a mathematical model. *Cancer Res.* **66**(14), 7293–7300 (2006)
7. G. Caravagna, A. d’Onofrio, P. Milazzo, R. Barbuti, Tumour suppression by immune system through stochastic oscillations. *J. Theor. Biol.* **265**(3), 336–345 (2010)
8. A. Cerwenker, L. Lanier, Natural killer cells, viruses and cancer. *Nat. Immunol.* 41–48 (2001)
9. M.A. Cheever, PROVENGE (Sipuleucel-T) in prostate cancer: the first FDA-approved therapeutic cancer vaccine. *Clin. Cancer Res.* **17**, 35203,526 (2011)
10. S.E. Clare, F. Nakhlis, J.C. Panetta, Molecular biology of breast cancer metastasis: The use of mathematical models to determine relapse and to predict response to chemotherapy in breast cancer. *Breast Cancer Res.* **2**, 430–435 (2000)
11. D. Cunningham, Y. Humblet, S. Siena, Cetuximab monotherapy and cetuximab plus irinotecan in irinotecan-refractory metastatic colorectal cancer. *N. Engl. J. Med.* **351**, 337–45 (2004)
12. L. de Pillis, D. Mallet, A. Radunskaya, Spatial tumor-immune modeling. *Comput. Math. Methods Med.* **7**(2–3), 159–176 (2006)
13. L. de Pillis, A. Radunskaya, H. Savage, Mathematical model of colorectal cancer with monoclonal antibody treatments. URL <http://arxiv.org/abs/1312.3023>. Preprint
14. L. de Pillis, A.E. Radunskaya, The dynamics of an optimally controlled tumor model: A case study. *Math. Comput. Model. (Special Issues)* **37**(11), 12211,244 (2003)
15. L.G. de Pillis, A.E. Radunskaya, A mathematical tumor model with immune resistance and drug therapy: An optimal control approach. *J. Theor. Med.* **3**, 79–100 (2001)
16. L.G., de Pillis, A.E. Radunskaya, C.L. Wiseman, A validated mathematical model of cell-mediated immune response to tumor growth. *Cancer Res.* **65**(17), 7950–7958 (2005)
17. V.J. De Vita, S. Hellman, S. Rosenberg, *Cancer: Principles and Practice of Oncology*, 7 edn. (Lippincott Williams & Wilkins, Sydney 2000)
18. A. Diefenbach, E.R. Jensen, A.M. Jamieson, D.H.: Rael, Rae1 and h60 ligands of the nkg2d receptor stimulate tumour immunity. *Nature* **413**(6852), 165–171 (2001)

19. A. d'Onofrio, A general framework for modeling tumor-immune system competition and immunotherapy: Mathematical analysis and biomedical inferences. *Phys. D* **208**(3), 220–235 (2005)
20. A. d'Onofrio, Metamodeling tumor-immune system interaction, tumor evasion and immunotherapy. *Math. Comput. Model.* **47**(5), 614–637 (2008)
21. A. d'Onofrio, A. Gandolfi, Resistance to antitumor chemotherapy due to bounded-noise-induced transitions. *Phys. Rev. E* **82**, 061,901 (2010)
22. C. DuBois, J. Farnham, E. Aaron, A. Radunskaya, A multiple time-scale computational model of a tumor and its micro environment. *MBE* **10**(1), 121–150 (2013)
23. M.E. Dudley, J.R. Wunderlich, P.F. Robbins, J.C. Yang, P. Hwu, D.J. Schwartzentruber, S.L. Topalian, R. Sherry, N.P. Restifo, A.M. Hübicki, M.R. Robinson, M. Raffeld, P. Duray, C.A. Seipp, L. Rogers-Freezer, K.E. Morton, S.A. Mavroukakis, D.E. White, S.A. Rosenberg, Cancer regression and autoimmunity in patients after clonal repopulation with antitumor lymphocytes. *Science* **298**(5594), 850–854 (2002)
24. O.K. Dzivenu, J. O'Donnell-Tormey, Cancer and the immune system: the vital connection. Online (2003). URL <http://www.cancerresearch.org/cancer-immunotherapy/resources/cancer-and-the-immune-system>
25. P. Ehrlich, Über den jetzigen stand der karzinomforschung. *Ned. Tijdschr. Geneesk.* **5**, 273–290 (1909)
26. A. Farrell, Milestone 3, (1909) Immune surveillance, hide and seek. *Nat. Med.* (2006)
27. S.C. Ferreira, M.L. Martins, M.J. Vilela, Reaction-diffusion model for the growth of avascular tumor. *Phys. Rev. E* **65**, 021,907 (2002)
28. J. Folkman, M. Hochberg, Self-regulation of growth in three dimensions. *J. Exp. Med.* **138**, 745–753 (1973)
29. C. Gravalos, J. Cassinello, P. Garcia-Alfonso, A. Jimeno, Integration of panitumumab into the treatment of colorectal cancer. *Crit. Rev. Oncol. Hematol.* **74**(1), 16–26 (2010)
30. H. Greenspan, Models for the growth of a solid tumor by diffusion. *Stud. Appl. Math.* **51**, 317–338 (1972)
31. A.M. Grothey, Defining the role of panitumumab in colorectal cancer. *Community Oncology* **3**, 10–16 (2006)
32. B.J. Kennedy, Cyclic leukocyte oscillations in chronic myelogenous leukemia during hydroxyurea therapy. *Blood* **35**(6), 751–760 (1970)
33. D.D. Kirschner, J.C. Panetta, Modeling immunotherapy of the tumor - immune interaction. *J. Math. Biol.* **37**(3), 235–252 (1998)
34. Krikorian, J., Portlock, C., Cooney, D., Rosenberg, S.: Spontaneous regression of non-hodgkin's lymphoma: A report of nine cases. *Cancer* **46**, 2093–2099 (1980)
35. N.N. Kronik, Y. Kogan, V. Vainstein, Z. Agur, Improving alloreactive ctl immunotherapy for malignant gliomas using a simulation model of their interactive dynamics. *Cancer Immunol. Immunother.* **57**(3), 425–439 (2008)
36. V. Kuznetsov, in *A Survey of Models for Tumor-Immune System Dynamics*, eds. by J. Adam, N. Bellomo Basic Models of Tumor-Immune System Interactions- Identification, Analysis and Predictions (Birkhauser, Basel 1997)
37. H.J. Lenz, Cetuximab in the management of colorectal cancer. *Biologics* **2**, 77–91 (2007)
38. A. Lin, A model of tumor and lymphocyte interactions. *Discrete Contin. Dyn. Syst. Ser. B* **4**(1), 241–266 (2004)
39. Mallett, D., de Pillis, L.: A cellular automata model of tumor-immunesystem interactions. *J. Theor. Biol.* **239**, 334–350 (2006)
40. E. Martinelli, R. De Palma, M. Orditura, F. De Vita, F. Ciardiello, Anti-epidermal growth factor receptor monoclonal antibodies in cancer therapy. *Clin. Exp. Immunol.* **158**, 1–9 (2009)
41. A. Matzavinos, M.A. Chaplain, V.A. Kuznetsov, Mathematical modelling of the spatio-temporal response of cytotoxic t-lymphocytes to a solid tumour. *Math. Med. Biol.* **21**(1), 1–34 (2004)
42. L. Norton, R. Simon, H. Brereton, A. Bogden, Predicting the course of gompertzian growth. *Nature* **264**, 542–545 (1976)

43. W. Paul, *Fundamental Immunology*, 5 edn. Lippincott, Williams and Wilkins Publishers, Sydney (2003)
44. A.S. Perelson, G. Weisbuch, *Immunology for physicists*. *Rev. Mod. Phys.* **69**, 1219–1268 (1997)
45. S. Pilon-Thomas, M., Verhaegen, J. Mulé, Dendritic cell-based therapeutics for breast cancer. *Heart Disease* **20**, 65–71 (2004)
46. O. Preynat-Seauve, E. Contassot, P. Schuler, L.E. French, B. Huard, Melanoma-infiltrating dendritic cells induce protective antitumor responses mediated by t cells. *Melanoma Res.* **17**, 169–176 (2007)
47. A. Radunskaya, S. Hook, in: *New Challenges for Cancer Systems Biomedicine* eds. by A. d’Onofrio, P. Cerrai, A. Gandolfi, Modeling the kinetics of the Immune Response (Springer, Newyork, 2012), pp. 267–282.
48. A. Radunskaya, L. de Pillis, A. Gallegos, A model of dendritic cell therapy for melanoma. *Front. Oncology* **3**(56), 223–228 (2013)
49. H. Riedel, in *The Cancer Handbook Wiley*, ed. by M. Alison Models for tumour growth and differentiations (New Jersey Institute of Technology, New Jersey 2004)
50. S.A. Rosenberg, J. Yang, S.L.E.A. Topalian, Treatment of 283 consecutive patients with metastatic melanoma or renal cell cancer using high-dose bolus interleukin 2. *JAMA* **271**, 907–913 (1994)
51. J. Schmollinger, R. Vonderhelde, K. Hoar, R. Vonderheide, K. Hoar, Maecker, B., J., F.S., H. Schultze, R. Soiffer, K. Jung, M. Kuroda, N. Letvin, E. Greenfield, M. Mihm, J. Kutok, G.Dranoff, Melanoma inhibitor of apoptosis protein (mi-iap) is a target for immune-mediated tumor destruction. *Proc. Natl. Acad. Sci. USA* **100**(6), 3398–3403 (2003)
52. J. Sherratt, M. Nowak, *Oncogenes, anti-oncogenes and the immune response to cancer*. *Proc. R. Soc. Lond. B* **248**, 261–271 (1992)
53. S. Siena, A. Sartore-Bianchi, F. Di Nicolantonio, J. Balfour, A. Bardelli, Biomarkers predicting clinical outcome of epidermal growth factor receptor-targeted therapy in metastatic colorectal cancer. *J. Natl. Cancer Inst.* **101**, 1–17 (2009)
54. R. Soiffer, T. Lynch, M. Mihm, K. Jung, C. Rhuda, J. Schmollinger, F. Hodi, L. Liebster, P. Lam, S. Mentzer, S. Singer, K. Tanabe, A. Cosimi, R. Duda, A. Sober, A. Bhan, J. Daley, D. Neuberg, G. Parry, J. Rokovich, L. Richards, J. Drayer, A. Berns, S. Clift, L. Cohen, R. Mulligan, G. Dranoff, Vaccination with irradiated autologous melanoma cells engineered to secrete human granulocyte macrophage colony-stimulating factor generates potent antitumor immunity in patients with metastatic melanoma. *Proc. Natl. Acad. Sci. USA* **95**, 13,141–13,146 (1998)
55. J. Speer, V. Petrosky, M. Retsky, R. Wardwell, A stochastic numerical model of breast cancer growth that simulates clinical data. *Cancer Res.* **44**, 41244,130 (1984)
56. C.O. Starnes, Coley’s toxins in perspective. *Nature* **357**, 11–12 (1992)
57. O. von Stryk, User’s guide for DIRCOL: A direct collocation method for the numerical solution of optimal control problems. *Lehrstuhl M2 Numerische Mathematik, Technische Universitaet Muenchen* (1999)
58. R.M. Sutherland, Cell and environment interactions in tumor microregions: the multicell spheroid model. *Science* **240**, 177–184 (1988)
59. R. Thomlinson, Measurement and management of carcinoma of the breast. *Clin. Radiol.* **33**(5), 481–493 (1982)
60. L. Zhang, J. Conejo-Garcia, D. Katsaros, P. Gimotty, M. Massobrio, G. Regnani, A. Makriannakis, H. Gray, K. Schlienger, M. Liebman, S. Rubin, G. Coukos, Intratumoral t cells, recurrence, and survival in epithelial ovarian cancer. *N. Engl. J. Med.* **348**(3), 203–213 (2003)